3-27-1995

Novel Kalman filtering method for the suppression of gyroscope noise effects in pointing and tracking systems

Marcelo C. Aigrain

Novel Kalman filtering method for the suppression of gyroscope noise effects in pointing and tracking systems

Marcelo C. Algrain, MEMBER SPIE
Douglas E. Ehlers
University of Nebraska–Lincoln
Department of Electrical Engineering
and
Center for Electro-Optics
Lincoln, Nebraska 68588-0511
E-mail: marcelo@gaucho.unl.edu

Abstract. A primary cause of degraded performance in pointing and tracking systems is the jitter in the line of sight. This jitter is caused by the residual angular motion of the stabilized platform within the system. A major contributor to this residual motion is the gyroscope noise. Thus, to reduce angular jitter, lower-noise gyroscopes are selected, generally at a premium cost. Another approach is to enhance the accuracy of the gyroscopes electronically (by suppressing measurement noise) before their outputs are fed into the stabilized platform control system. Optimal filtering techniques can be used for this purpose. The goal is to estimate the platform motion so that the calculated value is closer to the actual value than the measurement is. Enhanced performance is obtained at the expense of added complexity, but in many cases this approach may prove to be more economical than resorting to more precise and costly lower-noise gyroscopes. This paper presents a novel Kalman filtering method that provides more accurate angular motion estimates than the measured values. The effectiveness of this method is evaluated through a computer simulation case study. The simulation demonstrates that the new approach yields excellent 3-D angular velocity estimates, very small mean square estimation errors, and over a 5-to-1 improvement (in the mean-square sense) over angular velocity measurements obtained from three orthogonal gyroscopes. The enhanced 3-D angular velocity estimates can be fed into the platform stabilization control system rather than feeding raw gyroscope measurements, thus significantly reducing the contribution of gyroscope noise toward the overall jitter in a stabilized platform. This would permit a relaxation on gyroscope noise specifications, which could lead to substantial savings while maintaining the same error budget.

Subject terms: pseudolinear systems; Kalman filtering; gyroscopes; pointing and tracking.

Optical Engineering 34(10), 3016–3030 (October 1995).

1 Introduction

Sensing equipment, such as TV cameras, radars, and navigation instruments, is frequently carried by and operated in a moving vehicle, such as an airplane, that undergoes rotational motion. In such an environment, the equipment is commonly installed on a platform that is stabilized with respect to its mounting base. The gimbals within the platform generate a counterrotation equal in magnitude and opposite in direction to that of the base, maintaining the line of sight (LOS) of the sensor (the image from the camera) on a preselected object regardless of vehicle motion. This combined motion, sensor-to-base and base-to-object, is commonly referred to as angular jitter or residual motion (inertial).

In precision stabilization platforms, a major jitter contributor is the gyroscope noise. To reduce angular jitter, lower-noise gyroscopes are selected, generally at a premium cost. Another approach is to enhance the accuracy of the gyroscopes electronically (by suppressing measurement noise) before their outputs are fed into the stabilized platform control system.[1–3] Optimal estimation techniques, such as Kalman filtering, can be used for this purpose. The ability of the Kalman filter to produce more accurate values for measured variables is attributed to the use (in the computation of the estimate) of statistical information about the process that generated those variables, and about the noise in the measurements of those variables.[4–7] Furthermore, the filter incorporates knowledge about the system itself through a model of its dynamical characteristics. The goal is to assess the true angular motion of the platform base so that the estimated value is closer to the actual value than the measurement is. Enhanced performance is obtained at the expense of added complexity, but in some cases this approach may provide a cost-effective alternative to using higher-accuracy (and thus more expensive) gyroscopes.

Paper 38054 received May 26, 1994; revised manuscript received Mar. 27, 1995; accepted for publication Mar. 27, 1995.

In order to use Kalman filtering techniques, the angular motion dynamics need to be described. Euler's equations provide the required model.[8] They give a nonlinear set of differential equations relating the angular acceleration about one axis to the net torque applied to that axis, and to the product of angular velocity components about the other two axes orthogonal to the first. The nature of the system nonlinearities creates significant challenges in the implementation of the Kalman filter. In order to solve this complex problem, a novel method to estimate 3-D angular jitter is used in this paper. The key development in this new approach is representing a nonlinear system with a pseudolinear model that is mathematically equivalent. The concept is akin to nonlinear state transformations,[9] but is far more flexible, is easy to obtain, and allows one to construct more general models of nonlinear systems than direct nonlinear transformations. This approach allows us to apply the linear Kalman filter directly to the equivalent linear model. This results in a Kalman filtering method for nonlinear systems that is simple, accurate, and computationally efficient, and avoids many of the complexities created by the extended Kalman filter. An explanation of how to obtain mathematically equivalent representations follows.

2 Equivalent Pseudolinear Representation of Nonlinear Systems

In general, the development of nonlinear control systems entails some form of system linearization. This can be accomplished by calculating the Jacobian matrices about an operating condition,[10] by feedback linearization[11,12] or through special state-space transformations.[13–19] The approach developed in this paper does not require any of the above. Instead, a nonlinear system is systematically decomposed into linear and nonlinear components. The nonlinear terms are then redefined as a new set of state variables. This leads to an equivalent-system representation that has a linear form and is easy to obtain.

To show this development, consider a nonlinear system with the following general state-space form:

$$\dot{X}=AX+f(X)+g(X,U)+h(U) \ , \tag{1}$$

where

U = system input vector
X = $[x_1 \ x_2 \ \ldots \ x_n]^T$ = system state vector
A = $[A_1 \ A_2 \ \ldots \ A_n]^T$
f = $[f_1 \ f_2 \ \ldots \ f_n]^T$
g = $[g_1 \ g_2 \ \ldots \ g_n]^T$
h = $[h_1 \ h_2 \ \ldots \ h_n]^T$
A_i = row vector of constant coefficients
f_i = nonlinear operator with $i=1, \ldots, n$
g_i = nonlinear operator with $i=1, \ldots, n$
h_i = linear or nonlinear operator with $i=1, \ldots, n$.

The term AX in Eq. (1) contains linear operations within the nonlinear system, the term $f(X)$ embodies nonlinear functions of the states, the term $g(X,U)$ includes nonlinear combinations of the states and inputs, and the term $h(U)$ represents functions of the inputs alone. Then the individual elements of the state vector are given by the following set of first-order differential equations:

$$\begin{aligned}
\dot{x}_1 &= A_1X+f_1(X)+g_1(X,U)+h_1(U) \ , \\
\dot{x}_2 &= A_2X+f_2(X)+g_2(X,U)+h_2(U) \ , \\
&\vdots \\
\dot{x}_n &= A_nX+f_n(X)+g_n(X,U)+h_n(U) \ .
\end{aligned} \tag{2}$$

A mathematically equivalent representation of the previous set of nonlinear differential equations can be obtained by introducing the following set of variables:

$$\begin{aligned}
z_i &= f_i(X) && \text{with} \quad i=1, \ldots, n \ , \\
v_i &= g_i(X,U)+h_i(U) && \text{with} \quad i=1, \ldots, n \ , \\
w_i &= \dot{f}_i(X) && \text{with} \quad i=1, \ldots, n \ .
\end{aligned} \tag{3}$$

This yields the following expressions:

$$\begin{aligned}
\dot{x}_1 &= A_1X+z_1+v_1 \ , \\
\dot{x}_2 &= A_2X+z_2+v_2 \ , \\
&\vdots \\
\dot{x}_n &= A_nX+z_n+v_n \ , \\
\dot{z}_1 &= w_1 \ , \\
\dot{z}_2 &= w_2 \ , \\
&\vdots \\
\dot{z}_n &= w_n \ .
\end{aligned} \tag{4}$$

The previous representation, written in state-space form, yields the following vector expression:

$$\dot{X}_{eq}=A_{eq}X_{eq}+B_{eq}U_{eq} \ , \tag{5}$$

where

X_{eq} = $[x_1 \ \ldots \ x_n \quad z_1 \ \ldots \ z_n]^T=[X \ Z]^T$,
U_{eq} = $[v_1 \ \ldots \ v_n \quad w_1 \ \ldots \ w_n]^T=[V \ W]^T$,
A_{eq} = $\begin{bmatrix} A & I_n \\ [0] & [0] \end{bmatrix}$,
B_{eq} = I_{2n} = identity matrix of order $2n$.

Equation (5) has a linear form in terms of the vectors X_{eq} and U_{eq}, and it is mathematically equivalent to the original nonlinear system. A restriction in this development is that the first time derivative of the nonlinear function f_i needs to exist for $i=1, \ldots, n$.

The new state vector X_{eq} contains the actual nonlinear system state variables x_1 through x_n, and the pseudo-state-variables z_1 through z_n contain the system nonlinearities. The lack of nonlinear terms in some of the equations would reduce the number of auxiliary variables introduced, and the order of the augmented system would be less than $2n$.

Analogously to X_{eq}, the vector U_{eq} is formed using pseudoinputs v_i, which result from the relationships $g_i(X,U)$ and $h_i(U)$.

This variable substitution scheme leads to an augmented system that is mathematically equivalent to the original nonlinear system, but it has a linear form. The term *pseudolinear* is introduced to differentiate between a truly linear system and one that is artificially constructed through the introduction of new variables. This augmented equivalent linear system can be used along with conventional linear Kalman filtering designs, yielding a simple and effective estimation method for nonlinear systems.

Alternatively to directly filtering the augmented state vector, the vector formed by the true states and the vector formed by the pseudostates can be filtered separately. This approach, called *interlaced Kalman filtering* (IKF), is presented in Ref. 20, where a nonlinear estimation problem is solved without requiring complex linearization processes or extended Kalman filtering (EKF) techniques. This simplification is obtained at the expense of having to run two linear Kalman filters simultaneously. However, the IKF has the advantage over the EKF that the Kalman gains do not need to be continuously updated, significantly reducing the computational burden. This is because the system representation does not change with the operating states. This is not the case for the EKF, since the Jacobian matrices need to be recomputed every time the value for the state estimate changes. Then, a change in the Jacobian matrices would lead to computing a new set of Kalman gains. In addition, the EKF method involves a nonlinear projection of the estimate. This must be done through the nonlinear system dynamics. That is, we find the predicted value of the estimate $\hat{X}(t_{k+1})$ by solving $\dot{X}=f(X,U,t)$ at $t=t_{k+1}$, subject to the initial conditions $X=\hat{X}$ at $t=t_k$. In most cases, this is not trivial,[21] and it is not needed in the IKF approach.

In the preceding development, the system's nonlinear terms were split into the separate functions $f(X)$, $g(X,U)$, and $h(U)$, as shown in Eq. (1). This maintained separation between those terms associated with the states only, those associated with the inputs only, and those associated with both. Alternatively, these functions could be lumped into a single term, which could be treated as the input vector to the pseudolinear system. The advantage to this is that no additional states are introduced, and the order of the pseudolinear system is the same as that of the original nonlinear system. This simplification leads to a variation of the IKF method hereafter referred to as the *pseudolinear Kalman filter* (PLKF), which does not require a second Kalman filter running simultaneously. In this new approach, the general state-space form is given by

$$\dot{X}=AX+j(X,U) \ , \tag{6}$$

where j is now a nonlinear operator acting on the states and/or inputs. A mathematically equivalent representation of this nonlinear system can be obtained through the following substitution:

$$j(X,U)=U_D+U_S \ , \tag{7}$$

where U_D represents terms that are associated with the states and/or deterministic inputs, and U_S embodies the random inputs. The estimation of the system states can be accomplished analogously to the Kalman-filtering case with deterministic inputs.[22] To illustrate the PLKF process, consider the discrete-time case where the system and measurement models are described by

$$\begin{aligned} X(n+1)&=AX(n)+B_DU_D(n)+B_SU_S(n) \ , \\ Y(n)&=HX(n)+V(n), \end{aligned} \tag{8}$$

where

X = state vector
Y = measurement vector
U_D = deterministic pseudoinput
U_S = random input with covariance Q
V = measurement noise with covariance R
A = system matrix
B_D = deterministic input matrix
B_S = stochastic input matrix.

The mechanization of the PLKF process is realized by the execution of the following steps:

- *Step 0:* Assume initial state vector and error covariance:

  $\hat{X}(0|-1)=$ assumed value ,

  $P(0|-1)=$ assumed value .

- *Step 1:* Calculate Kalman gains:

  $K(n)=P(n|n-1)H^T[HP(n|n-1)H^T+R(n)]^{-1}$.

- *Step 2:* Compute new state vector:

  $\hat{X}(n)=\hat{X}(n|n-1)+K(n)[Y(n)-H(n)\hat{X}(n|n-1)]$.

- *Step 3:* Update error covariance estimate:

  $P(n)=[I-K(n)H]P(n|n-1)$.

- *Step 4:* Propagate state vector and error covariance:

  $\hat{X}(n+1|n)=A\hat{X}(n)+B_DU_D(n)$,

  $P(n+1|n)=AP(n)A^T+B_SQ(n)B_S^T$.

- *Step 5:* Make new measurement and repeat from step 1 for new time index.

The particulars for the application of the PLKF method to 3-D angular motion estimation follow.

3 The Pseudolinear Kalman Filtering Algorithm for the Estimation of 3-D Angular Motion

In the case of 3-D angular motion, the system dynamics are described by Euler's equations of motion. Expressing that motion along the body's principal axes of inertia leads to the following expressions[23]:

$$\dot{\omega}_1=\frac{I_2-I_3}{I_1}\omega_2\omega_3+\frac{M_1}{I_1} \ ,$$

$$\dot{\omega}_2=\frac{I_3-I_1}{I_2}\omega_1\omega_3+\frac{M_2}{I_2}\ ,$$
$$\dot{\omega}_3=\frac{I_1-I_2}{I_3}\omega_1\omega_2+\frac{M_3}{I_3}\ , \tag{9}$$

where

I_1 = principal moment of inertia about roll axis
I_2 = principal moment of inertia about pitch axis
I_3 = principal moment of inertia about yaw axis
M_1 = random torque applied to roll axis
M_2 = random torque applied to pitch axis
M_3 = random torque applied to yaw axis
ω_1 = body angular velocity along roll axis
ω_2 = body angular velocity along pitch axis
ω_3 = body angular velocity along yaw axis
$\dot{\omega}_1$ = body angular acceleration along roll axis
$\dot{\omega}_2$ = body angular acceleration along pitch axis
$\dot{\omega}_3$ = body angular acceleration along yaw axis.

The system of equations (9) provides a set of nonlinear differential equations, known as Euler's equations, that completely defines the angular motion of a rigid body in 3-D space. To use them as system model for the discrete Kalman filter they need to be expressed as difference equations. This can be accomplished using a variety of forms, but for sufficiently small time intervals an angular acceleration can be approximated with a first forward difference between angular velocities, as follows:

$$\dot{\omega}(n)\approx\frac{\omega(n+1)-\omega(n)}{\delta t}\ , \tag{10}$$

where

$\dot{\omega}(n)$ = angular acceleration at time index n
$\omega(n+1)$ = angular velocity at time index $n+1$
$\omega(n)$ = angular velocity at time index n
δt = incremental time step.

Substituting Eq. (10) into Eq. (9), and after some manipulations, the following state-space representation for the discrete-time progression of 3-D angular velocities is obtained:

$$X_\omega(n+1)=X_\omega(n)+B_DU_D(n)+B_SU_S(n)\ ,$$
$$Y_\omega(n)=X_\omega(n)+V_\omega(n)\ , \tag{11}$$

where

X_ω = $[\omega_1\ \omega_2\ \omega_3]^T$
U_D = $X_Z=[z_1\ z_2\ z_3]^T=f(X_\omega)=[\omega_2\omega_3\ \omega_1\omega_3\ \omega_1\omega_2]^T$
U_S = $[M_1\ M_2\ M_3]^T$ = random torque disturbances
V_ω = $[v_1\ v_2\ v_3]^T$ = angular velocity measurement noise,

and the matrices B_D and B_S are defined as follows:

$$B_D=\begin{bmatrix}\delta t\frac{I_2-I_3}{I_1} & 0 & 0\\ 0 & \delta t\frac{I_3-I_1}{I_2} & 0\\ 0 & 0 & \delta t\frac{I_1-I_2}{I_3}\end{bmatrix}\ ,$$

$$B_S=\begin{bmatrix}\frac{\delta t}{I_1} & 0 & 0\\ 0 & \frac{\delta t}{I_2} & 0\\ 0 & 0 & \frac{\delta t}{I_3}\end{bmatrix}\ .$$

The vector U_D is composed of the pseudo-state-variables, which contain the nonlinearities. It becomes a deterministic input to the model describing the progression of angular velocities. To complete the overall pseudoequivalent model, the means for propagating the nonlinearities (products of angular velocities) need to be devised. The state vector containing the nonlinearities was defined as

$$X_Z=[z_1\ z_2\ z_3]^T=[\omega_2\omega_3\ \omega_1\omega_3\ \omega_1\omega_2]^T\ . \tag{12}$$

Differentiating each element in Eq. (12) leads to the following relationships:

$$\dot{z}_1=\omega_3\dot{\omega}_2+\omega_2\dot{\omega}_3\ ,$$
$$\dot{z}_2=\omega_3\dot{\omega}_1+\omega_1\dot{\omega}_3\ , \tag{13}$$
$$\dot{z}_3=\omega_2\dot{\omega}_1+\omega_1\dot{\omega}_2\ .$$

Using the first-difference approximations for continuous time derivatives in Eq. (13) (forward difference on the left-hand side and backward difference on the right-hand side of the equations) leads to the following state-space representation for the progression in time of products of orthogonal angular velocity components:

$$X_Z(n+1)=X_Z(n)+U'_D(n)+U'_S(n)\ , \tag{14}$$

where

U'_D = $F[X_\omega(n), X_\omega(n-1)]=[F_1\ F_2\ F_3]^T$
F_1 = $[\omega_2(n)-\omega_2(n-1)]\omega_3(n)-[\omega_3(n)-\omega_3(n-1)]\omega_2(n)$
F_2 = $[\omega_1(n)-\omega_1(n-1)]\omega_3(n)-[\omega_3(n)-\omega_3(n-1)]\omega_1(n)$
F_3 = $[\omega_1(n)-\omega_1(n-1)]\omega_2(n)-[\omega_2(n)-\omega_2(n-1)]\omega_1(n)$
U'_D = random term that forces the equality to hold.

Equation (14) gives a linear model for the propagation of the state vector X_Z. This model contains a nonlinear function of the state vector X_ω, but it is linear in terms of the state vector X_Z, thus complying with the linearity criteria with respect to the pseudo-state-variables. This is a key consideration in developing a pseudolinear Euler equivalent model.

In order to treat the vectors U_D and U'_D as deterministic inputs to their respective system models, they should be obtained separately. The IKF method makes this possible. Equations (11) and (14) provide the discrete-time models to be

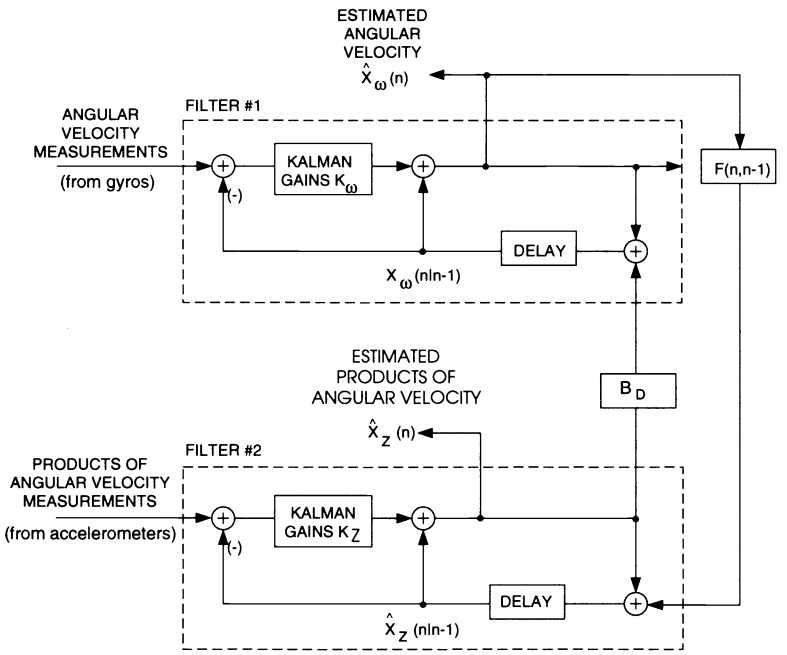

Fig. 1 Block diagram of interlaced Kalman filter.

used by each of the filters. The filtering process is illustrated in Fig. 1. The first filter estimates orthogonal angular velocity components, and the second estimates their products (taken two at a time). The measurements used by the first filter are provided by angular rate sensors (gyros). Another set of independent measurements is supplied to the second filter. The product of angular velocity components (taken two at a time) can be sensed by an arrangement of linear accelerometers.[24] This measurement scheme is illustrated in Fig. 2. Point O represents the rotational center of a vehicle around which the angular velocity $\omega=[\omega_1\ \omega_2\ \omega_3]^T$ is exerted. Linear accelerometers placed at points A, B, C, and D provide the following outputs: A_A^X, A_A^Y, A_A^Z, A_B^Y, A_B^Z, A_C^X, A_C^Z, A_D^X, and A_D^Y, where A_D^Y is the acceleration at point D in the Z direction, and likewise for the other outputs. Also, since the positions of the accelerometer with respect to each other ($R_{B/A}$, $R_{C/A}$, and $R_{D/A}$) are known, all the necessary data are readily available to obtain independent measurements for the products of angular velocity components, as follows:

$$\omega_1\omega_2=\frac{A_B^Y-A_A^Y}{2R_{B/A}}+\frac{A_C^X-A_A^X}{2R_{C/A}}\ ,$$

$$\omega_1\omega_3=\frac{A_B^Z-A_A^Z}{2R_{B/A}}+\frac{A_D^X-A_A^X}{2R_{D/A}}\ , \tag{15}$$

$$\omega_2\omega_3=\frac{A_C^Z-A_A^Z}{2R_{C/A}}+\frac{A_D^Y-A_A^Y}{2R_{D/A}}\ .$$

Since the product of angular velocity components can be measured as a linear combination of accelerometer outputs, whatever noise is in the accelerometers will be reflected as additive noise in the overall measurements. Furthermore, if the accelerometer noise is Gaussian, the noise in the measurements for angular velocity products will also be Gaussian,

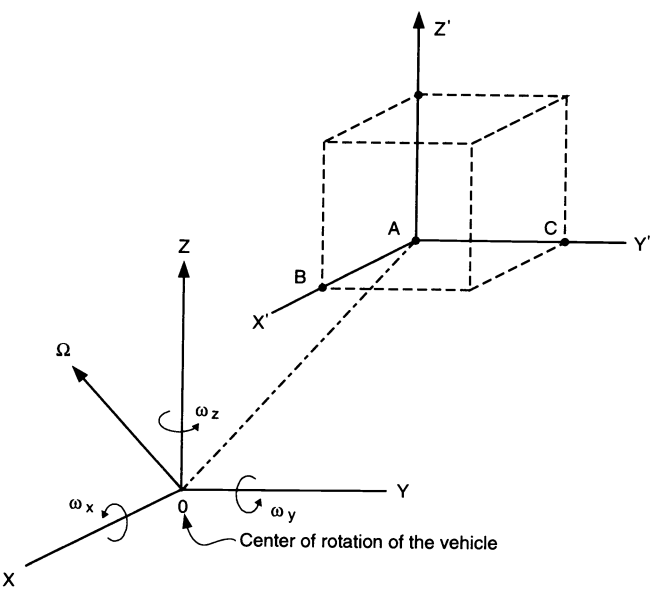

Fig. 2 Linear accelerometer arrangement for angular motion determination.

since it results from linear combinations of Gaussian-distributed noises.

We now have separate models describing the dynamics of angular velocities and their products [Eqs. (11) and (14)], and independent measurements for angular velocities (from gyros) and products of angular velocity components (from accelerometers). Furthermore, we can assume that the measurement noises are Gaussian, and that the random disturbances U_S and U_S' are Gaussian as well. Under these assumptions the linear Kalman filter becomes the optimal filter.[25] As a trade-off between optimality and practicality, let us replace the independent measurements provided by the

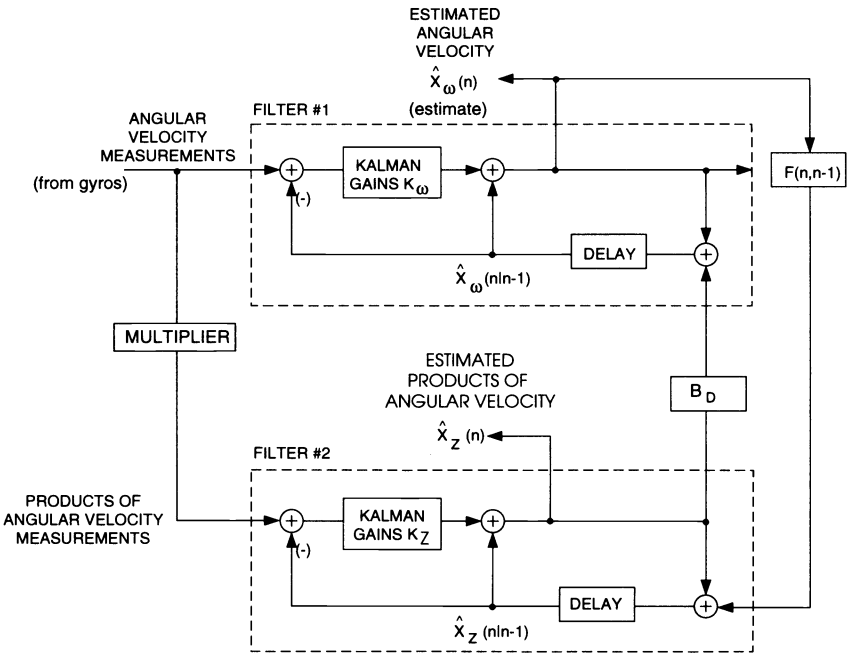

Fig. 3 Block diagram of modified interlaced Kalman filter.

accelerometers with algebraic manipulations on the gyro outputs. In other words, the measurements for products of angular velocity components are now obtained by multiplying angular velocity measurements. The resulting IKF process is illustrated by Fig. 3. The issue now is the characterization of the measurement noise under the proposed algebraic-measurement scheme.

To address this issue let us consider the measurement equation. Assuming the additive Gaussian noise v_i in the angular velocity measurements, the measurement equations can be expressed as

$$Y_{\omega_i}(n)=\omega_i(n)+v_i(n) \qquad \text{for} \quad i=1,2,3 \ . \tag{16}$$

Then the measurement equations for the product of angular velocities are given by

$$\begin{aligned} Y_{Z_1}(n)&=Y_{\omega_2}(n)Y_{\omega_3}(n) \ , \\ Y_{Z_2}(n)&=Y_{\omega_1}(n)Y_{\omega_3}(n) \ , \\ Y_{Z_3}(n)&=Y_{\omega_1}(n)Y_{\omega_2}(n) \ . \end{aligned} \tag{17}$$

Now the statistical characteristics of the products of random processes need to be analyzed. For this purpose, let x and y be two random processes defining a third random process $z=xy$. Then the system $xy=z$ and $x=w$ has a single solution, namely $x=w$ and $y=z/w$. Hence, the probability density function of the random variable $z=xy$ is given by (see Ref. 26)

$$p_Z(z)=\int_{-\infty}^{\infty}\frac{1}{|w|}p_{XY}\left(w,\frac{z}{w}\right)\,dw \ . \tag{18}$$

From the nature of the angular velocity estimation problem, it is reasonable to assume that the random variables corresponding to angular velocities are independent (due to the orthogonality between axes) and Gaussian-distributed, and that the measurement noises are also independent (a common assumption). Then

$$p_Z(z)=\int_{-\infty}^{\infty}\frac{1}{|w|}p_X(w)p_Y\left(\frac{z}{w}\right)\,dw \ . \tag{19}$$

The analytical solution of Eq. (19) is rather involved. For that reason, a numerical approach is used instead. The variables x and y are generated using the random number generator of the XMATH software.[27] The distribution is Gaussian with zero mean and standard deviation of one. A total of 8192 (2^{13}) points are generated for each variable. The random variable z is generated through point-by-point multiplication. The probability density function of z can be defined as

$$p_Z=\lim_{\Delta z\to 0,\ N\to\infty}\frac{N_Z}{\Delta z\, N} \ , \tag{20}$$

where

Δz = incremental step size on z
N_Z = relative frequency of occurrence for z
N = total number of occurrences for z.

For a sufficiently small step size, p_Z can be approximated[28] by the histogram of z. That is, p_Z can be obtained graphically by plotting the normalized relative frequency of z versus itself. This is shown in Fig. 4, where the histogram envelope is plotted for $\Delta z=0.03$. It is clear from this figure that the resulting distribution of z is not Gaussian. However, the random process $z(t)$ is still white, since[29] $z(t_i)$ is uncorrelated with $z(t_j)$ for every $t_i\neq t_j$. A plot of autocorrelation function is provided in Fig. 5. Note that the experimentally obtained

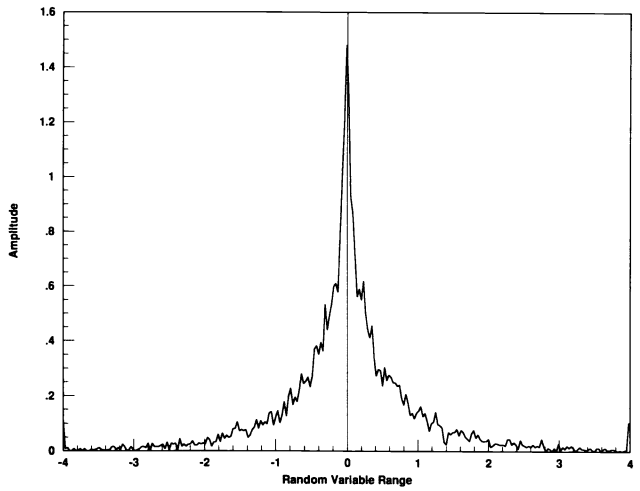

Fig. 4 Probability density for product of two Gaussian processes.

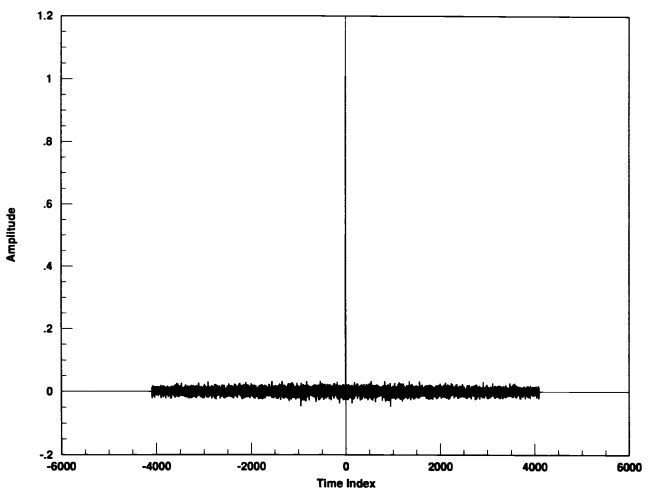

Fig. 5 Autocorrelation function for product of two Gaussian processes.

autocorrelation function $R_Z(t_i,t_j)$ is approximately equal to $1.0\delta(t_i-t_j)$, with δ a delta function. This confirms that a random process generated by multiplying two Gaussian-distributed random variables is white. As long as the processes are white, the Kalman filter can be validly applied. In fact, the Kalman filter is the optimal linear estimator if the random process is white, and it is the optimal estimator if the process is Gaussian.[30] Therefore, the IKF method provides an optimal linear estimation approach for solving the problem of nonlinear angular velocity estimation. This approach is simpler than the EKF method in that it does not require the continuous update of the Jacobian matrices, nor the nonlinear propagation of the state estimate. This simplification is obtained at the expense of having to run two separate linear Kalman filters, but it is less computationally intensive than the EKF method, since the nonlinear projection of the state estimate is avoided.

As a further trade-off between optimality and practicality, let us replace the second linear Kalman filter (estimating the nonlinear terms, i.e., products of angular velocity components) with a nonlinear operator acting on the estimates of the first Kalman filter. This constitutes the pseudolinear Kalman filter (PLKF), which is schematically shown in Fig. 6. Then the pseudolinear model describing the discrete-time progression of 3-D angular velocities is given by

$$\begin{aligned} X_\omega(n+1) &= X_\omega(n) + B_D U_D(n) + B_S U_S(n) \ , \\ Y_\omega(n) &= X_\omega(n) + V_\omega(n) \ , \end{aligned} \tag{21}$$

where

X_ω = $[\omega_1 \ \omega_2 \ \omega_3]^T$ = angular velocity vector

U_D = $f(\hat{X}_\omega) = [\hat{\omega}_2\hat{\omega}_3 \ \hat{\omega}_1\hat{\omega}_3 \ \hat{\omega}_1\hat{\omega}_2]^T$ = nonlinear terms

U_S = $[M_1 \ M_2 \ M_3]^T$ = random torque disturbances

V_ω = $[v_1 \ v_2 \ v_3]^T$ = angular velocity measurement noise

$\hat{X}_\omega$ = $[\hat{\omega}_1 \ \hat{\omega}_2 \ \hat{\omega}_3]^T$ = PLKF estimate of angular velocity vector.

Equation (21) provides a linear discrete-time Euler equivalent model that can be used to estimate stabilized platform motion (as a 3-D angular velocity) using the pseudolinear Kalman filter. The result is a filtering technique that allows one to estimate 3-D angular motion in a robust, computationally efficient, and accurate manner. In fact, it is shown in Sec. 5 that results yielded by the PLKF are indistinguishable from those obtained using the IKF and EKF methods. Then, the more accurate values of platform motion obtained by this method can be used as inputs to the stabilization control system (rather than feeding the raw measurements) to reduce the contribution of gyroscope noise to the overall jitter in a stabilized platform. A description of a stabilization system implementing this approach is presented in the section that follows.

4 LOS Stabilization System Description

The direction in which one must look to obtain an image is called the line of sight (LOS). Stabilizing the image is equivalent to stabilizing its LOS. In the general case of a three-axis stabilization system, such as the one schematically shown in Fig. 7, the stabilization of the LOS is accomplished by actuating the gimbals to generate a relative motion equal in magnitude and opposite in direction to that of the base

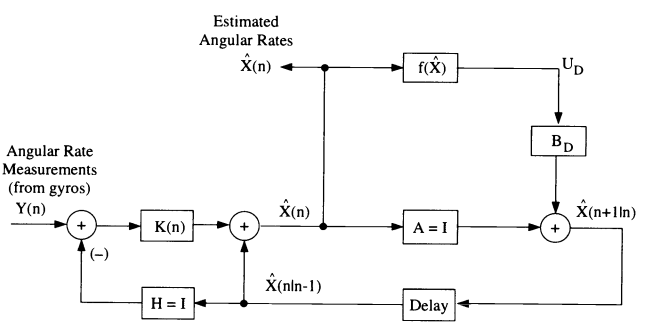

Fig. 6 Pseudolinear Kalman filter for 3-D angular motion estimation.

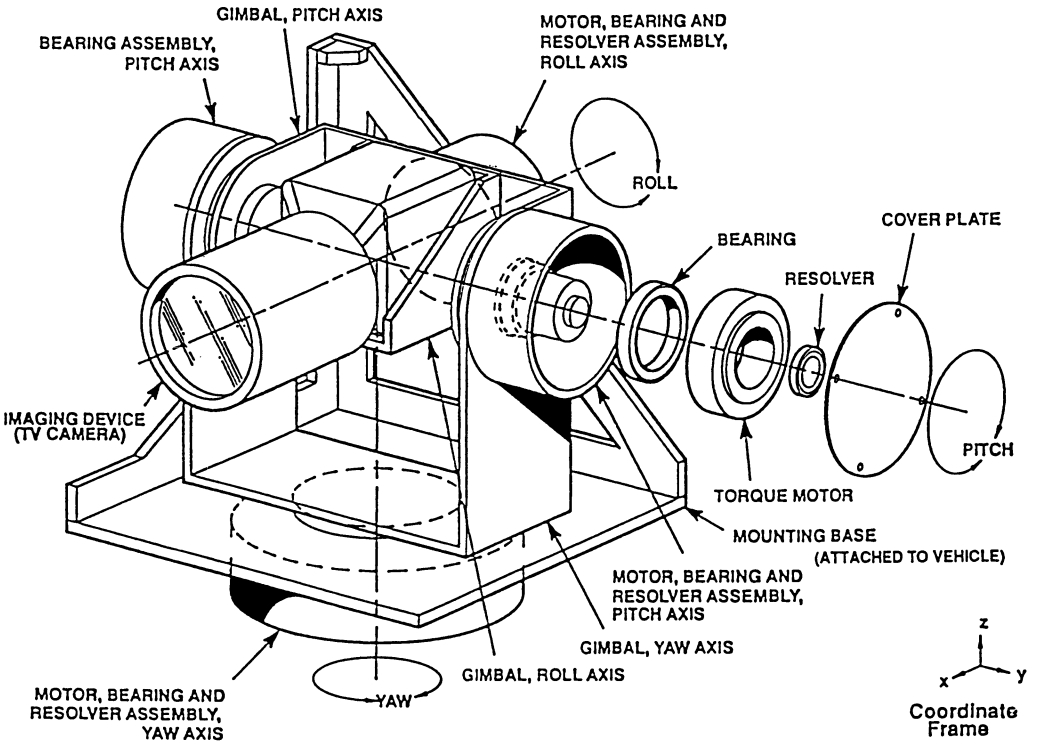

Fig. 7 Three-axis stabilization system.

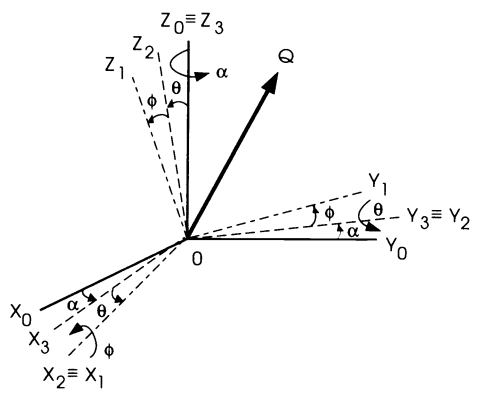

Fig. 8 Multiple rotating frames.

motion. The interdependence between rotating frames within the gimbal system is shown in Fig. 8. The frame $X_0Y_0Z_0$ corresponds to the mounting base, $X_3Y_3Z_3$ corresponds to the yaw gimbal (outer rotation), $X_2Y_2Z_2$ corresponds to the pitch gimbal, and $X_1Y_1Z_1$ corresponds to the roll gimbal (inner rotation). The LOS is represented by the vector $\mathbf{Q}$. For the LOS to be stabilized, i.e., not moving, the rate of change of that vector must be zero ($\dot{\mathbf{Q}}=\mathbf{0}$). This *stabilization criterion* can be mathematically expressed by projecting all the angular velocity vectors onto a common frame and equating the result to zero, as follows:

$$\mathbf{0}=\omega_1\mathbf{i}_0+\omega_2\mathbf{j}_0+\omega_3\mathbf{k}_0+\omega_R\mathbf{i}_1+\omega_P\mathbf{j}_2+\omega_Y\mathbf{k}_3 \ , \tag{22}$$

where

$\omega_1, \omega_2, \omega_3$ = base roll, pitch, and yaw rates, respectively

$\omega_R, \omega_P, \omega_Y$ = gimbal roll, pitch, and yaw rates, respectively

$\mathbf{i}_0, \mathbf{j}_0, \mathbf{k}_0$ = orthogonal unit vectors for base frame

$\mathbf{i}_1, \mathbf{j}_2, \mathbf{k}_3$ = unit vectors for roll, pitch, and yaw gimbal axes, respectively.

For convenience, all vectors are projected onto the mounting-base coordinate frame. The relationships between the unit vectors within the gimbal system and the base are shown in Fig. 9. From these relationships, the unit vectors $\mathbf{i}_1, \mathbf{j}_2, \mathbf{k}_3$ can be expressed in terms of $\mathbf{i}_0$, $\mathbf{j}_0$, and $\mathbf{k}_0$, as follows:

$$\begin{aligned}
&\mathbf{k}_3=\mathbf{k}_0 \ , \\
&\mathbf{j}_2=\mathbf{j}_3=-\sin\alpha\ \mathbf{i}_0+\cos\alpha\ \mathbf{j}_0 \ , \\
&\mathbf{i}_1=\mathbf{i}_2=\cos\theta\ \mathbf{i}_3-\sin\theta\ \mathbf{k}_3 \\
&\qquad =\cos\theta\ \cos\alpha\ \mathbf{i}_0+\cos\theta\ \sin\alpha\ \mathbf{j}_0-\sin\theta\ \mathbf{k}_0 \ .
\end{aligned} \tag{23}$$

Substituting the equations in (23) into Eq. (22) allows us to calculate the roll, pitch, and yaw gimbal rates required to stabilize the LOS, as shown below:

$$\begin{aligned}
\omega_R &= -\frac{\omega_1+\omega_2\ \tan\alpha}{\cos\theta\ \cos\alpha+\tan\alpha\ \cos\theta\ \sin\alpha} \ , \\
\omega_P &= -\frac{\omega_2+\omega_R\ \cos\theta\ \sin\alpha}{\cos\alpha} \ , \\
\omega_Y &= -\omega_3+\omega_R\ \sin\theta \ .
\end{aligned} \tag{24}$$

The equations in (24) give the velocity setpoints for the roll, pitch, and yaw servo motors. These variables are fed as

inputs to the speed control system, commanding the servomotors to rotate the gimbals at the speeds required to stabilize the LOS. The variables ω_1, ω_2, and ω_3 are measured using three orthogonal gyroscopes. The noise in these measurements incorporates errors into the setpoint calculations, which increases the LOS jitter. This effect can be suppressed using the PLKF method. The enhanced 3-D angular velocity estimates of the jitter can be fed into the platform stabilization control system rather than feeding raw gyroscope measurements; this significantly reduces the contribution of gyroscope noise toward the overall jitter in a stabilized platform. The advantage of this technique is that it facilitates the relaxation of gyroscope noise specifications, which can lead to substantial savings, while maintaining the same error budget. This approach is schematically shown in Fig. 10.

5 Computer Simulation Results

The performance of the PLKF-enhanced stabilization system is evaluated in this section through a computer simulation case study. In order to generalize the results, all variables have been scaled to a platform having unitary inertia with respect to one of its axes. The normalized angular rates for the base motion are assumed to be random, with Gaussian distribution, variance 0.1, mean zero, and bandlimited to 10 Hz. These angular velocities are plotted in Figs. 11(a), 12(a), and 13(a), corresponding to the roll, pitch, and yaw rates, respectively. Three orthogonal gyroscopes are used to sense these rates, providing measurements that are corrupted with white Gaussian noise with mean zero and variance 0.1. This scenario creates a condition of low signal-to-noise ratio to be improved by the Kalman filter. The measured angular rates are shown in Figs. 11(b), 12(b), and 13(b), corresponding to the roll, pitch, and yaw axes, respectively.

The PLKF method was used to estimate the actual angular velocities [shown in Figs. 11(a) to 13(a)] based on the noisy measurements available [shown in Figs. 11(b) to 13(b)]. The results are provided in Figs. 14(b), 15(b), and 16(b), corresponding to the estimated angular rates for the roll, pitch, and yaw axes of the base. To ease the comparison, the plots for actual roll, pitch, and yaw rates are repeated in Figs. 14(a), 15(a), and 16(a), respectively. It can be concluded from these figures that the estimated rates provide excellent estimates of the actual rates, in spite of the very low signal-to-noise ratio imposed. This is further attested by comparing the estimation errors with the measurement noise. The estimation errors are plotted in Figs. 17(a), 18(a), and 19(a), corresponding to the roll, pitch, and yaw axes, respectively. The corresponding gyroscope measurement noises are provided in Figs. 17(b), 18(b), and 19(b), respectively. It is evident from these figures that the gyroscope noise has been effectively suppressed. This is confirmed by the mean-square-error (MSE) calculation results shown in Table 1, corresponding to the average of the results obtained for 70 Monte Carlo experiments. The standard deviation corresponding to the MSE data is provided in Table 2. Since the standard deviations for these data are so small, high statistical confidence can be placed in these results.

Taking the ratio between the estimated and measured values in Table 1 leads to the conclusion that the PLKF method yields over a 5-to-1 accuracy improvement in the estimated versus measured values of angular rates (in the mean-square sense). These enhanced estimates of platform base motion can be used in the gimbal rate setpoint determination [Eq. (25)] to improve the accuracy of the calculations, ultimately yielding lower LOS jitter. This is demonstrated by the simulation results shown in Figs. 20 through 22. In these figures, the rates for the residual motion (jitter) of the stabilized element within the platform are given. Figure 20(a) shows the residual roll rate of the stabilized element when the PLKF estimated rates are used in the setpoint calculations according to Eq. (24). Figure 20(b) shows the residual roll rate when the raw measurements are used in the setpoint calculations. Likewise, Figs. 21 and 22 show equivalent results for the pitch and yaw axes, respectively. These figures clearly show that a significant improvement is obtained using the PLKF method. This is further attested by the mean-square values of the residual angular rates for each axis given in Table 3. These results represent the average of 70 Monte Carlo experiments. The standard deviations corresponding to these data are given in Table 4. Once more, the standard deviations are very small, and high statistical confidence can be placed in these results.

In short, the simulation results embodied in Figs. 20–22 and Table 3 demonstrate that the mean-square residual motion of the stabilized element within the platform can be reduced by nearly a factor of 5 when the PLKF estimates are used in the calculation of gimbal rate setpoints, instead of directly using the angular rates measured by orthogonal gyroscopes mounted at the base of the stabilized platform. This may allow a relaxation in gyroscope noise specifications that

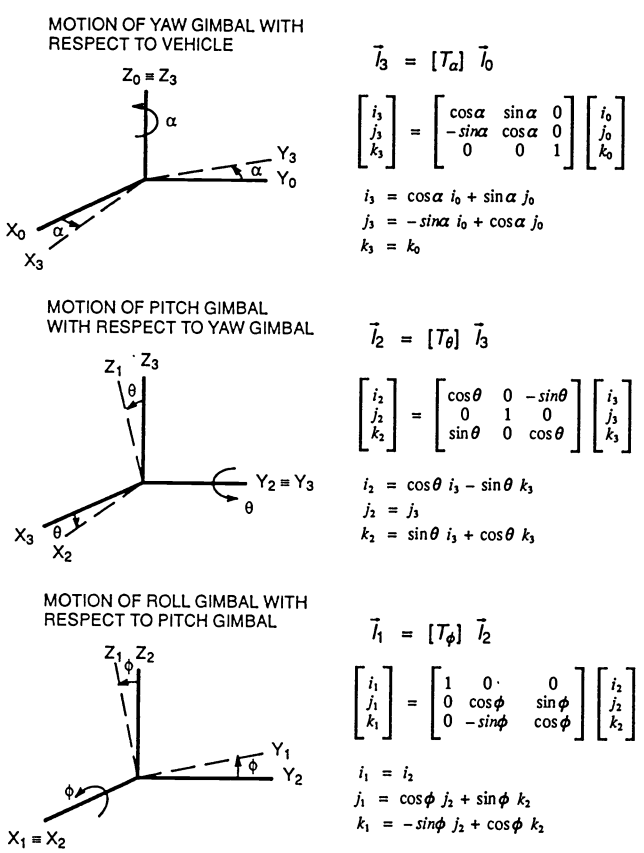

Fig. 9 Relationships between rotating frames.

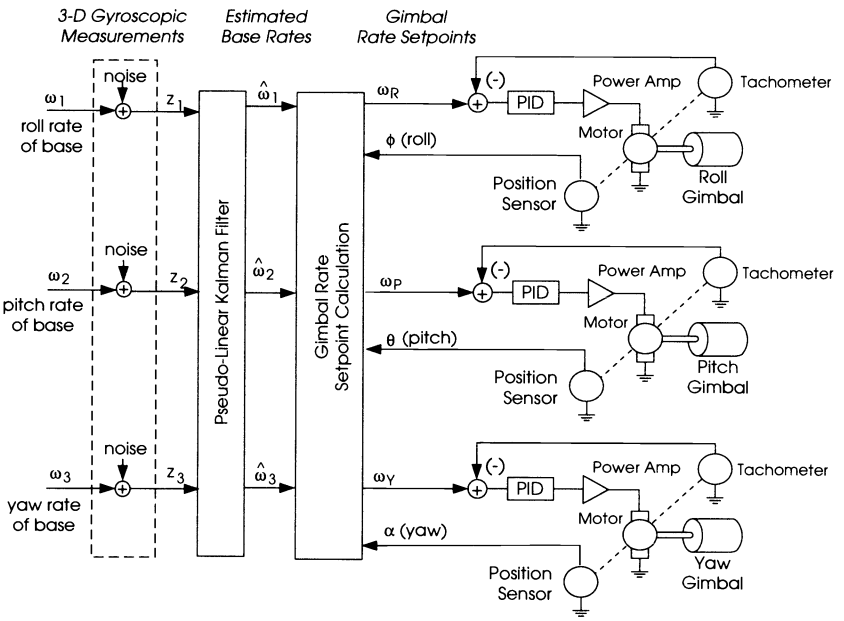

Fig. 10 Overall system diagram.

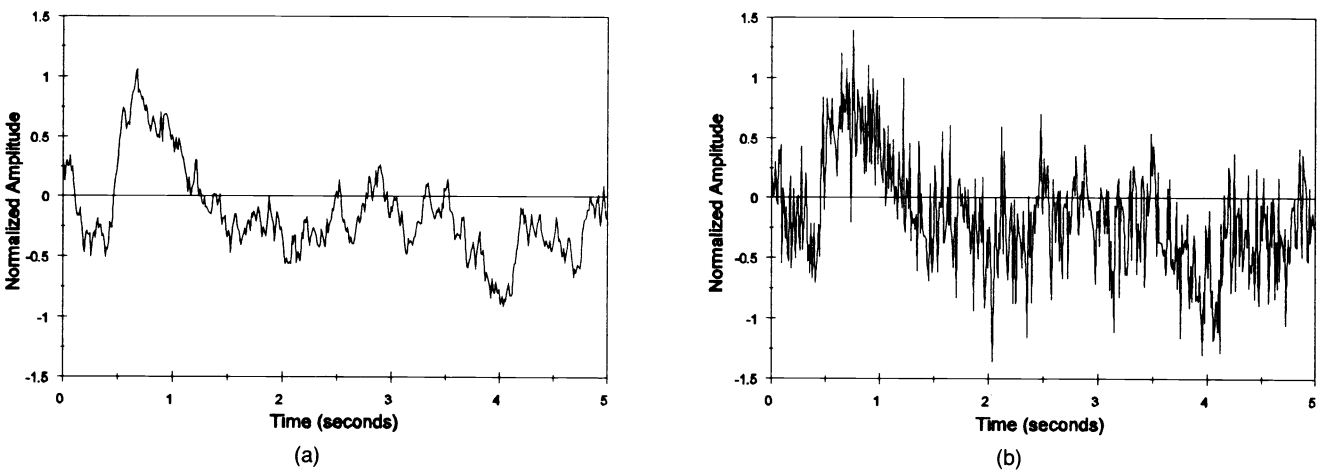

Fig. 11 (a) Actual roll rate; (b) roll-rate measurement.

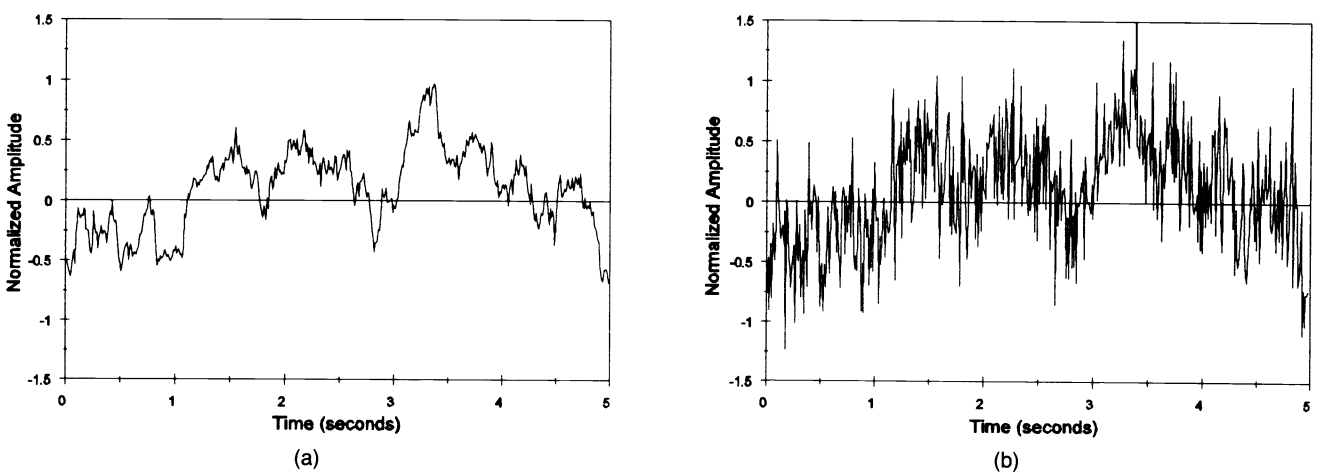

Fig. 12 (a) Actual pitch rate; (b) pitch-rate measurement.

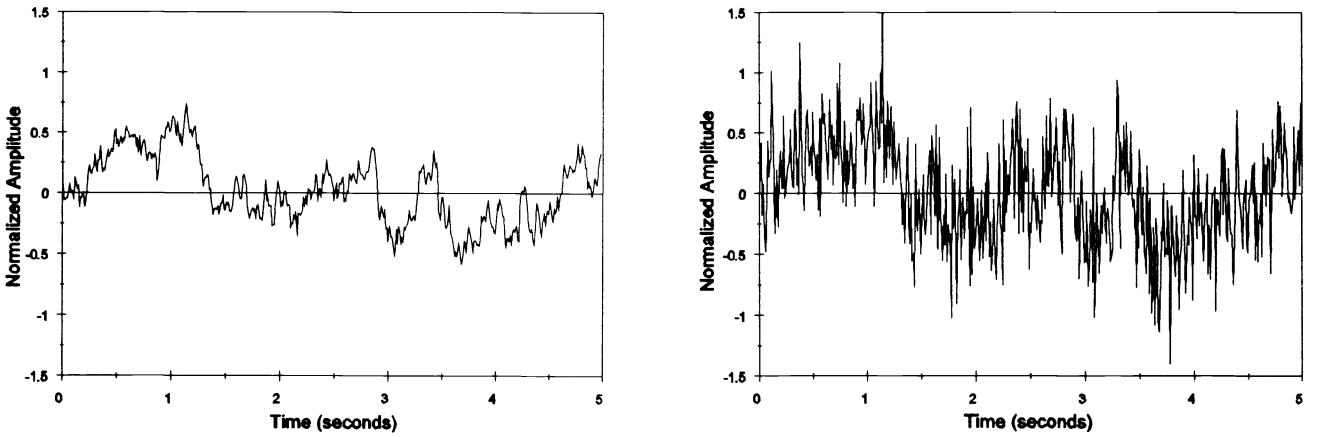

Fig. 13 (a) Actual yaw rate; (b) yaw-rate measurement.

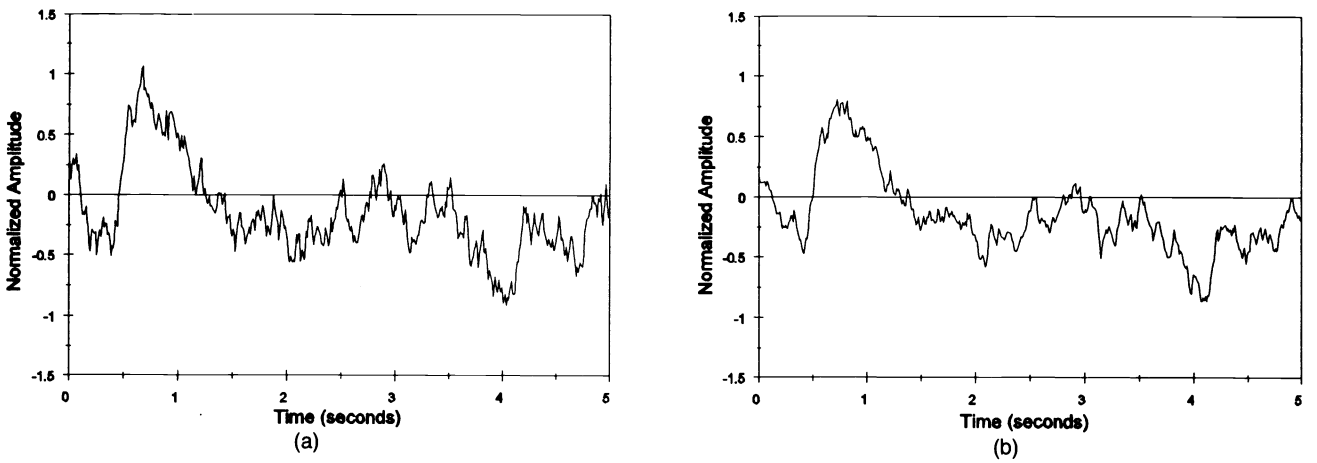

Fig. 14 (a) Actual roll rate; (b) roll-rate estimate.

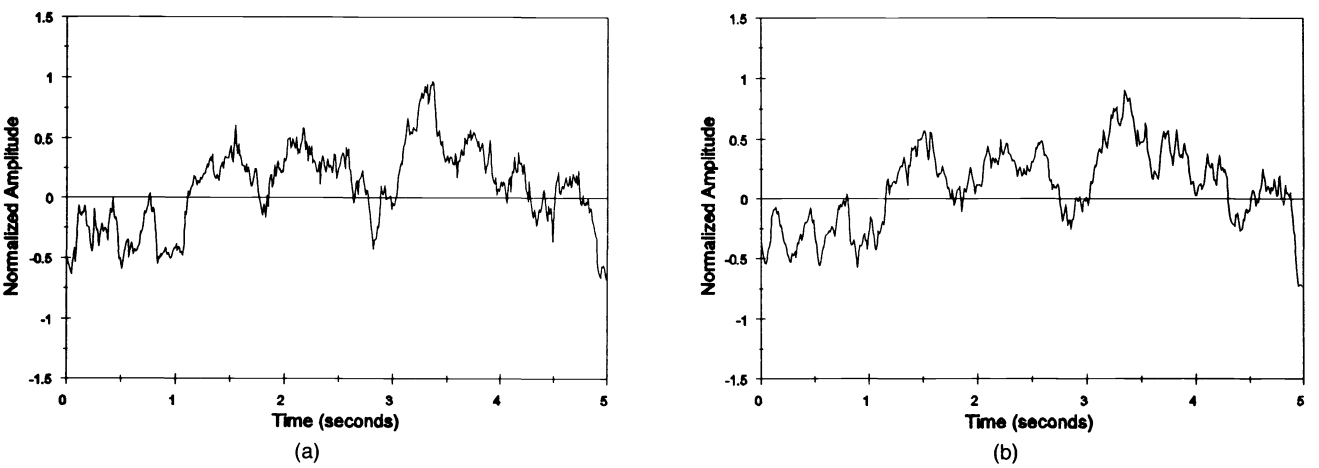

Fig. 15 (a) Actual pitch rate; (b) pitch-rate estimate.

Table 1 Calculated mean-square estimation errors.

	PLKF	Measured
Roll Axis	0.02063	0.11139
Pitch Axis	0.02025	0.11138
Yaw Axis	0.02079	0.11045

Table 2 Standard deviation of mean-square estimation errors.

	PLKF	Measured
Roll Axis	0.00272	0.00454
Pitch Axis	0.00263	0.00436
Yaw Axis	0.00202	0.00427

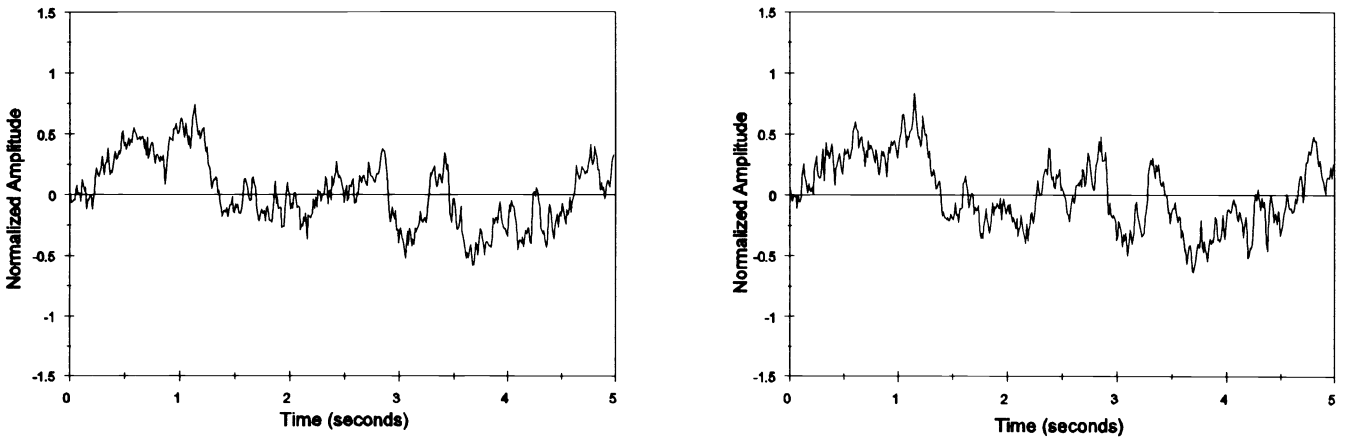

Fig. 16 (a) Actual yaw rate; (b) yaw-rate estimate.

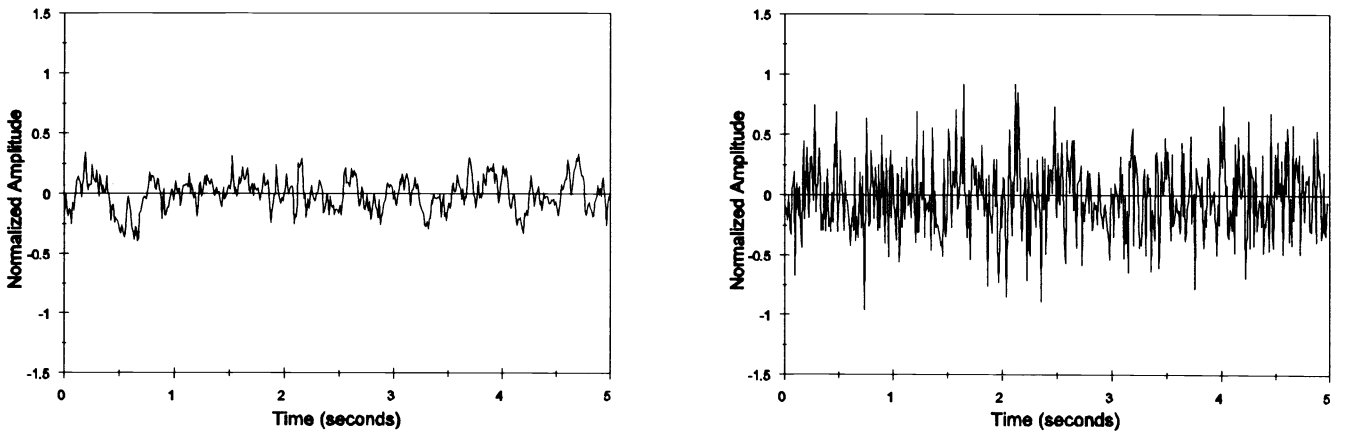

Fig. 17 (a) Roll-rate estimation error; (b) roll-rate measurement noise.

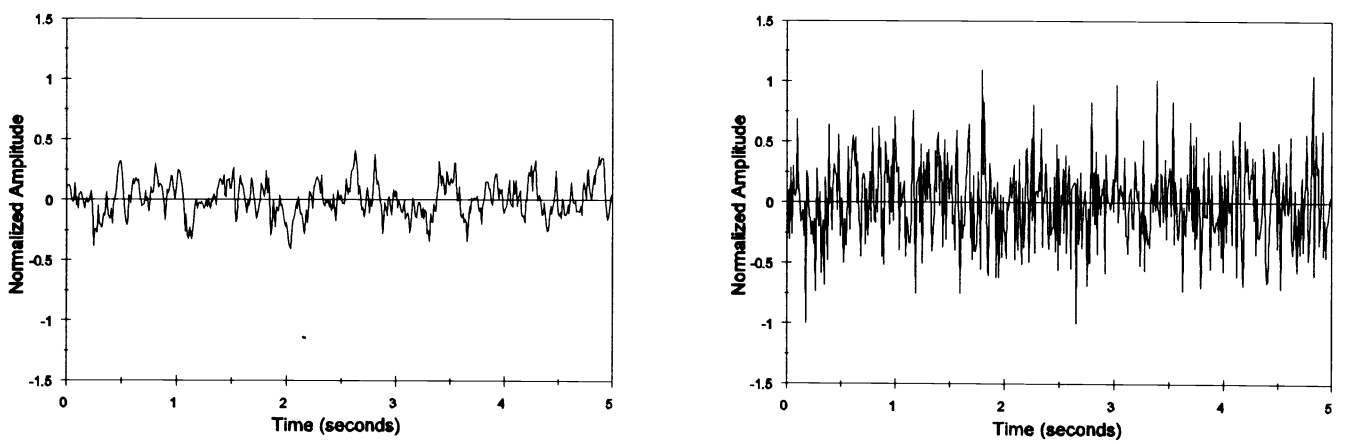

Fig. 18 (a) Pitch-rate estimation error; (b) pitch-rate measurement noise.

Table 3 Calculated mean-square residual angular rates.

	Using PLKF	Using Measurement
Roll Axis	0.02167	0.10717
Pitch Axis	0.02092	0.11714
Yaw Axis	0.02165	0.11663

Table 4 Standard deviation for mean-square residual angular rates.

	Using PLKF	Using Measurement
Roll Axis	0.00288	0.03090
Pitch Axis	0.00273	0.01307
Yaw Axis	0.00207	0.03645

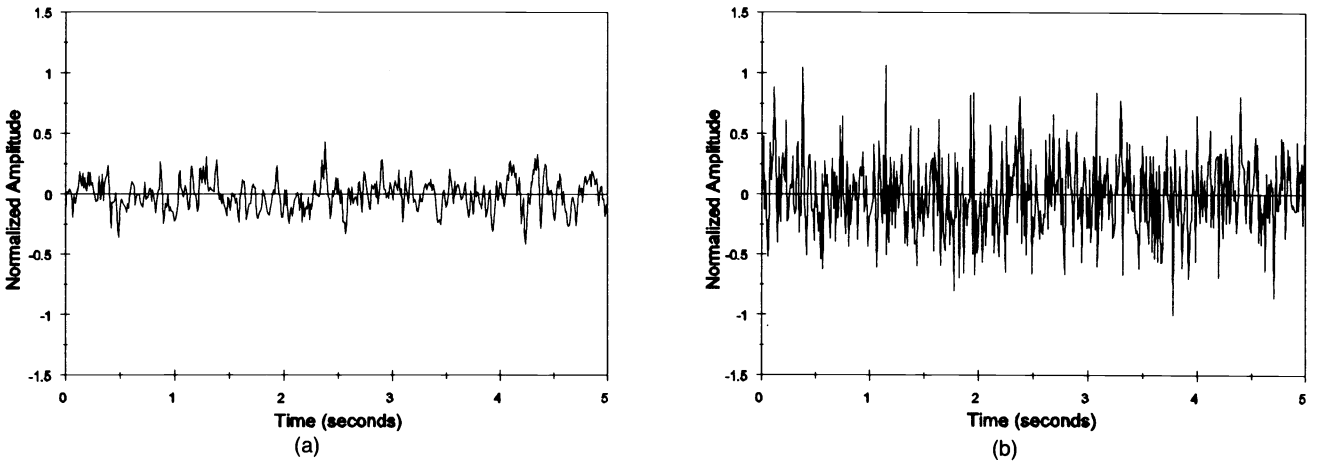

Fig. 19 (a) Yaw-rate estimation error; (b) Yaw-rate measurement noise.

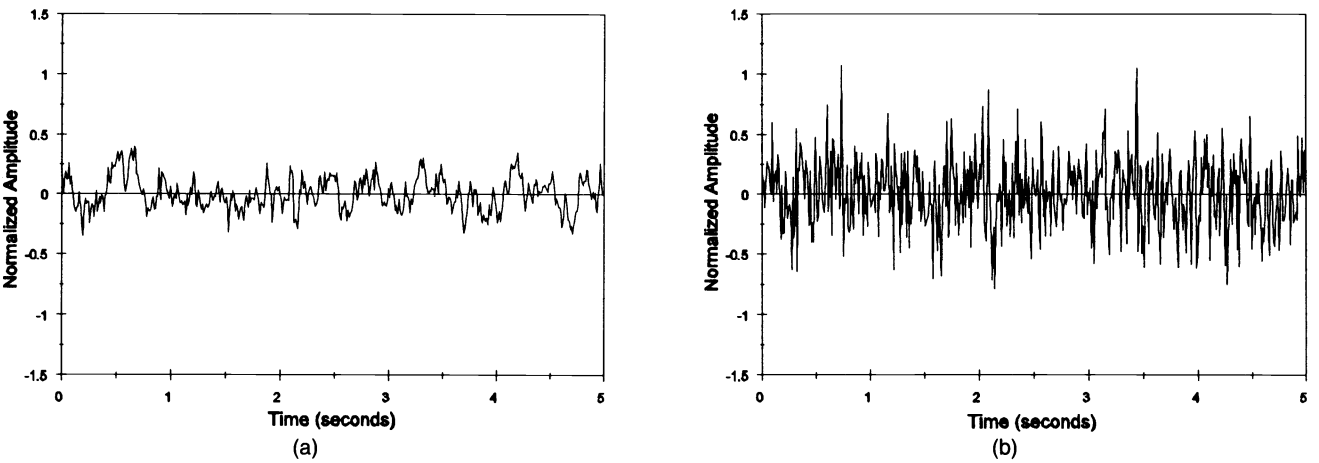

Fig. 20 Roll jitter (a) using estimate; (b) using measurement.

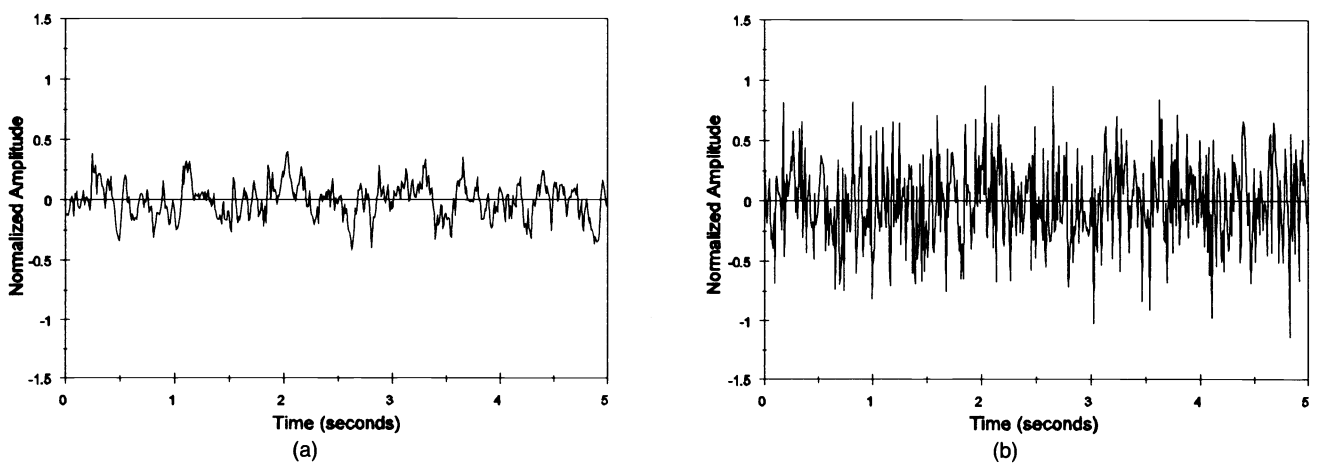

Fig. 21 Pitch jitter (a) using estimate; (b) using measurement.

could lead to significant savings. Furthermore, in spite of the considerably reduced complexity achieved by the PLKF method, the estimation accuracy and the results produced by the PLKF are indistinguishable from those yielded by the IKF and EKF methods.

6 Summary and Conclusions

This paper presents a novel optimal estimation method used to suppress angular jitter caused by noisy gyroscope measurements. The technique, called PLKF, produces excellent estimates of 3-D angular rates. The estimation improvements

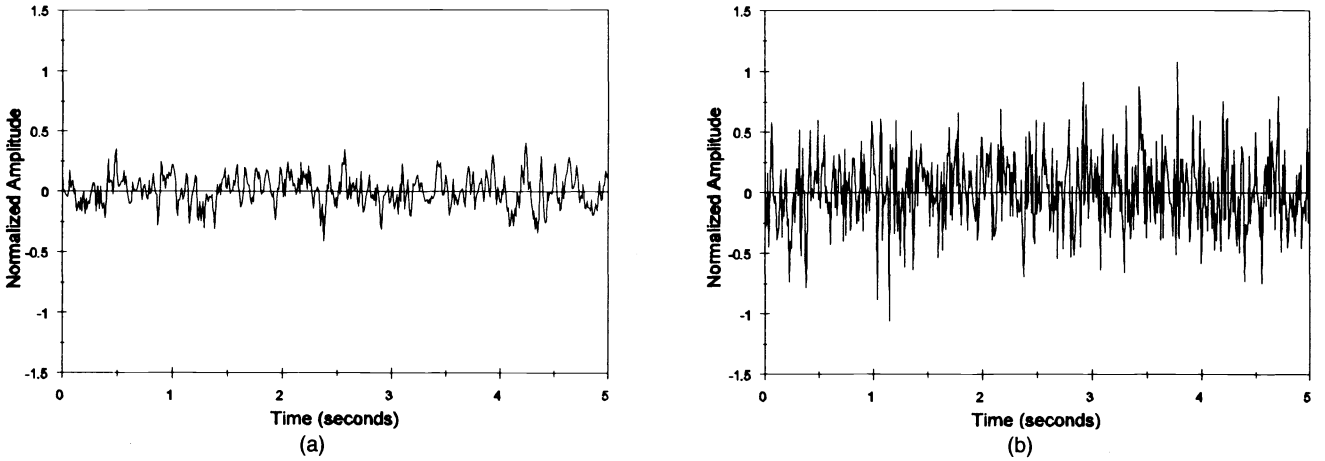

Fig. 22 Yaw jitter (a) using estimate; (b) using measurement.

over the measurements are demonstrated in a computer simulation case study. The example examines the effectiveness of the estimation method under the difficult scenario where the signal and noise are comparable in magnitude (low signal-to-noise ratio). The improvements obtained over the direct measurements are on the order of 5 to 1 (in the mean-square sense). The enhanced angular rates are then used (instead of raw gyroscopic measurements) to calculate the gimbal speeds required to stabilize the LOS. These variables are used as setpoints for the speed control system regulating the operation of the gimbals. This leads to a 5-to-1 reduction in the mean-square angular rates (jitter) observed at the stabilized element of the platform. This improvement is significant, and it could result in the loosening of gyroscope noise specifications, which could translate into considerable savings.

References

1. M. West and C. McCullough, "Optimal recursive filter for the attitude determination of the Spacelab instrument pointing subsystem," in *Proc. 28th IEEE Conf. on Decision and Control,* pp. 1800–1802, Tampa, FL (Dec. 1989).
2. C. Jayaraman and B. Class, "On-board attitude determination for the Explorer platform satellite," in *Proc. AAS/AISS Astrodynamics Conf.,* pp. 783–800, Durango, CO (Aug. 1991).
3. L. Stimac and T. Kennedy, "Sensor alignment Kalman filters for inertial stabilization systems," in *IEEE 1992 Position Location and Navigation Symp.—PLANS'92,* pp. 321–334, Monterey, CA (Mar. 1992).
4. A. Gelb, *Applied Optimal Estimation,* Chap. 4, MIT Press, Cambridge, MA (1974).
5. T. Kailath, Chapter 6 in *Lectures in Wiener and Kalman Filtering,* Springer-Verlag, New York (1981).
6. G. Minkler and J. Minkler, Chapter 7 in *Theory and Application of Kalman Filtering,* Magellan, Palm Bay, FL (1993).
7. H. Sorenson, *Kalman Filtering: Theory and Applications,* IEEE Press, New York (1985).
8. F. Beer and E. Johnston, *Vector Mechanics for Engineers,* 4th ed., Sec. 18.6, McGraw-Hill, New York (1984).
9. M. Vidyasagar, Chapter 7 in *Nonlinear Systems Analysis,* 2nd ed., Prentice-Hall, Englewood Cliffs, NJ (1993).
10. A. Isidori, Chapter 1 in *Nonlinear Control Systems,* 2nd ed., Springer-Verlag (1989).
11. J. Slotine and W. Li, Chapter 6 in *Applied Nonlinear Control,* Prentice-Hall, Englewood Cliffs, NJ (1991).
12. H. Nijmeijer and A. J. van der Schaft, Chapter 6 in *Nonlinear Dynamical Control Systems,* Springer-Verlag, Berlin, 1990.
13. G. Meyer, R. Su, and L. Hunt, "Application of nonlinear transformations to automatic flight control," *Automatica* **20**(1), 103–107 (1984).
14. L. Hunt and R. Villareal, "Canonical coordinates for partial differential equations," *Systems Control Lett.* **11,** 159–165 (1988).
15. M. Fliess, "Generalized controller canonical forms for linear and nonlinear dynamics," *IEEE Trans. Automat. Control,* pp. 994–1001 (Sep. 1990).
16. H. J. Sussmann and P. V. Kokotovic, "The peaking phenomenon and the global stabilization of nonlinear systems," *IEEE Trans. Automat. Control,* pp. 424–440 (Apr. 1991).
17. A. Isidori and J. Grizzle, "Fixed modes and nonlinear noninteracting control with stability," *IEEE Trans. Automat. Control,* pp. 907–914 (Oct. 1988).
18. C. I. Byrnes and A. Isidori, "Asymptotic stabilization of minimum phase nonlinear systems," *IEEE Trans. Automat. Control,* pp. 1122–1137 (Oct. 1991).
19. J. W. Grizzle, M. D. DiBenedetto, and F. Lamnabhi-Lagarrigue, "Necessary conditions for asymptotic tracking in nonlinear systems," *IEEE Trans. Automat. Control,* pp. 1782–1794 (Sep. 1994).
20. M. C. Algrain, and J. Saniie, "Interlaced Kalman filtering of 3-D angular motion using Euler's nonlinear equations," *IEEE Trans. Aerospace Electron Systems* **30**(1), 175–185 (Jan. 1994).
21. R. Brown and P. Hwang, Section 5.7.2 in *Introducton to Random Signals and Applied Kalman Filtering,* Wiley, New York (1991).
22. C. Chui and G. Chen, *Kalman Filtering,* Springer-Verlag, Berlin (1987).
23. A. D'Souza and V. Garg, *Advanced Dynamics, Modeling and Analysis,* Prentice-Hall, Englewood Cliffs, NJ (1984).
24. M. Algrain, "Gyroless line-of-sight stabilization for pointing and tracking systems," *Opt. Eng.* **33**(4), 1255–1260 (Apr. 1994).
25. J. Candy, Chapter 4 in *Signal Processing,* McGraw-Hill, New York (1986).
26. A. Papulis, *Probability, Random Variables, and Stochastic Processes,* 3rd ed., p. 147, McGraw-Hill, New York (1991).
27. *XMATH Reference Manual,* Integrated Systems, Inc., Santa Clara, CA (June 1994).
28. A. Breipohl, Section 8.6 in *Probabilistic Systems Analysis,* Wiley, New York (1970).
29. A. Papulis, *Probability, Random Variables, and Stochastic Processes,* 3rd ed., p. 295, McGraw-Hill, New York (1991).
30. F. Lewis, Section 2.3 in *Optimal Estimation,* Wiley-Interscience, New York (1986).

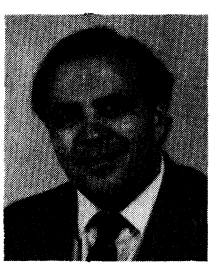

Marcelo C. Algrain received a BSME in 1980 and an MSEE in 1981, both from Wright State University, and a PhD in electrical engineering from the Illinois Institute of Technology in 1991. Since 1991 he has been an assistant professor at the University of Nebraska–Lincoln (UNL). From 1989 to 1991, he held the position of engineering specialist at Recon/Optical, Inc., where he performed analyses on stabilization and control systems for high-resolution reconnaissance systems. From 1984 to 1989, he was with Borg-Warner Research, developing control-system prototypes for a variety of automotive and industrial products. Prior to that, he was with Babcock & Wilcox, designing process control systems for nuclear power plants. Dr. Algrain is a member of SPIE, IEEE, and

AIAA. He has published numerous papers in the control-system field and holds two patents. His research interests are in stabilization; pointing and tracking systems; and stochastic, optimal, and adaptive controls.

Douglas E. Ehlers received a BSME in 1991 and an MSEE in 1995, both from the University of Nebraska–Lincoln. He is currently a development engineer at Transcrypt International in Lincoln, Nebraska. During 1992 he was employed by 3M in Wahpeton, ND, in the data storage products division as a process engineer. He has also interned with Phillips Petroleum of Bartlesville, OK, in both the mechanical design and computer network operations groups. He is a member of IEEE and ASME. His research interests are in controls, instrumentation, and microprocessors.